Supporting Information

Lee et al. 10.1073/pnas.1402243111

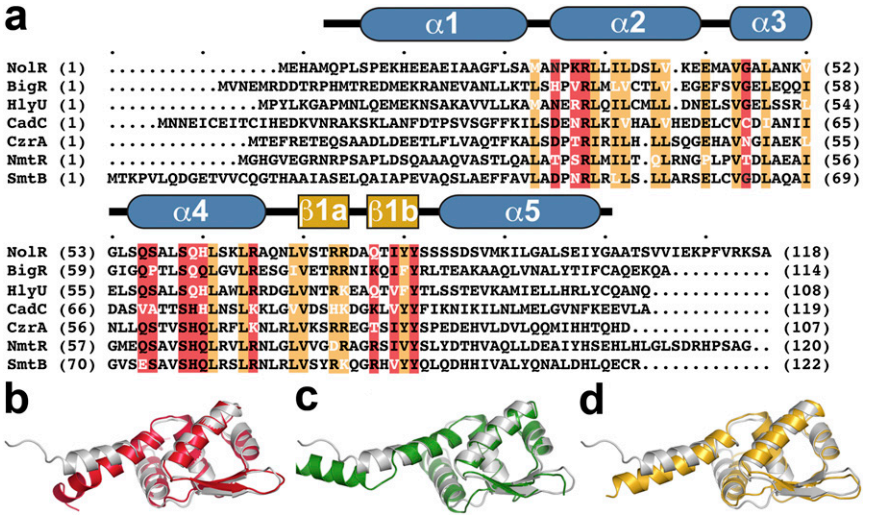

Fig. S1. Sequence and structure comparison of NolR and ArsR/SmtB transcription factors. (*A*) Multiple amino acid sequence alignment of *Sinorhizobium fredii* NolR (AAO27299.1), *Xylella fastidiosa* biofilm growth-associated repressor BigR (Q9PFB1.1), *Vibrio cholerae* HlyU (P52695.1), *Lactococcus lactis* CadC (P0A4U3.1), *Bacillus subtilis* CzrA (O31844.1), *Mycobacterium tuberculosis* NmtR (O69711.3), and *Synechococcus elongatus* SmtB (P30340.1). α-Helices (blue) and β-strands (gold) of NolR are indicated above the alignment. Protein–DNA interaction residues are highlighted in red and other conserved residues are indicated in orange. (*B–D*) Pairwise structural comparisons of NolR (gray) with (*B*) BigR (red, PDB ID code 3PQJ), (*C*) CadC (green, PDB ID code 3F72), and (*D*) HlyU (gold, PDB ID code 3JTH). Proteins structurally related to NolR were identified using the DALI server (http://ekhidna.biocenter.helsinki.fi/dali_server/) with overlays performed in COOT using the SSM Superimpose feature to align the models based on Cα positions.

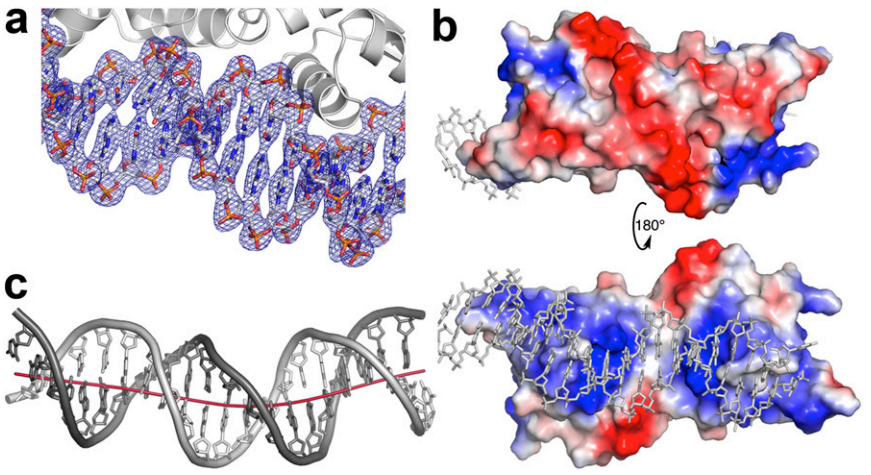

Fig. S2. Overview of DNA binding to NolR. (*A*) Representative final electron density ($2F_o - F_c$ map; 1.5 σ) of oligo AT bound to NolR. (*B*) Electrostatic surface potential of NolR. The surface of the homodimer is negatively charged (red) on the face opposite the DNA binding sites and presents a positively charged (blue) surface for interaction with DNA. Electrostatic surfaces were generated using the Adaptive Poisson-Boltzmann Server (APBS) program implemented in PyMOL. (*C*) NolR binding results in 16.8° bend in the DNA duplex compared with ideal B-form DNA. The curvature of oligo AT (red line) bound to NolR was calculated using 3D-DART.

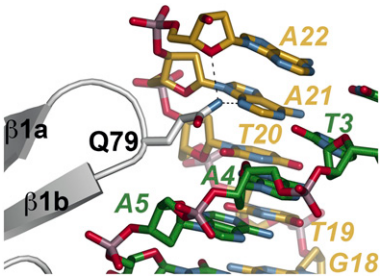

Fig. S3. Protein–DNA interaction in the minor groove of NolR in complex with oligo AT DNA. Nucleotides of the 5′ strand (gold) and 3′ strand (green) are shown as stick models. Portions of the wing β-sheet are shown as a ribbon diagram with the side-chain of Gln79 shown as a stick model. Hydrogen bond interactions are indicated by dotted lines.

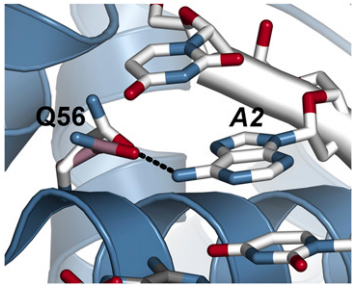

Fig. S4. Comparison of Gln56 positioning in the first interaction site of the NolR oligo AT and oligo AA structures. The structures of NolR in complex with oligos AT and AA were overlaid. The secondary structure features of the NolR•oligo AT complex are shown (blue). The phosphate backbone and nucleotides of oligoAT are shown (white). The structure of NolR complexed with oligo AA was similar and is not shown for clarity. The side-chain positions of Gln56 in the oligo AT (white) and oligo AA (rose) structures are shown as stick models. The hydrogen bond interaction between Gln56 and A2 is indicated by the dotted line.

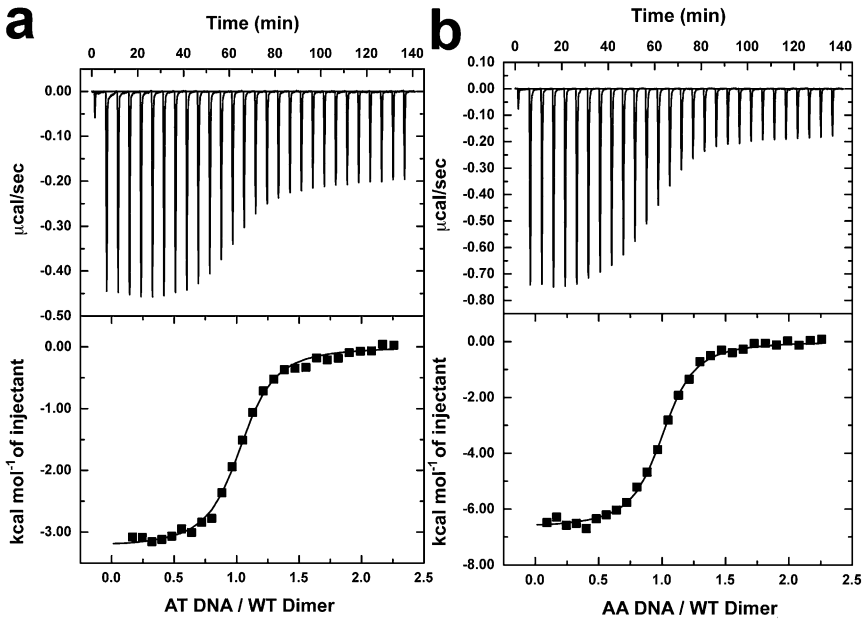

Fig. S5. Analysis of NolR–DNA interaction by isothermal titration calorimetry. Titrations of the NolR with (*A*) oligo AT and (*B*) oligo AA are shown. In each panel, the *Upper* window shows the isothermal titration calorimetry (ITC) data plotted as heat signal ($\mu cal \cdot s^{-1}$) versus time (min) for interaction of NolR with the DNA. The *Lower* window shows the integrated heat response per injection from titrations of NolR, with DNA plotted as normalized heat per mole of injectant.

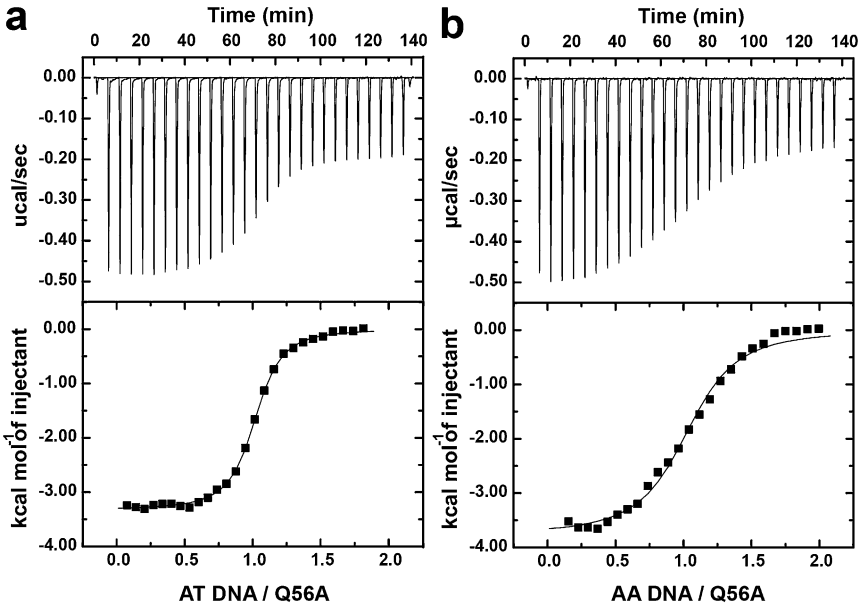

Fig. S6. Analysis of NolR Q56A mutant DNA interaction by isothermal titration calorimetry. Titrations of the NolR Q56A mutant with (*A*) oligo AT and (*B*) oligo AA are shown. In each panel, the *Upper* window shows the ITC data plotted as heat signal ($\mu cal \cdot s^{-1}$) versus time (min) for interaction of NolR Q56A with the DNA. The *Lower* window shows the integrated heat response per injection from titrations of NolR Q56A, with DNA plotted as normalized heat per mole of injectant.

Table S1. Summary of crystallographic statistics

	NolR (SeMet) oligo AT DNA	NolR uncomplexed	NolR oligo AA DNA
Data collection			
Space group	$P3_1$	C2	$P3_1$
Cell dimensions	$a = b = 131.0$ Å, $c = 67.69$ Å	$a = 99.77$ Å, $a = 99.62$ Å, $c = 113.0$ Å; $\beta = 90.1°$	$a = b = 131.3$ Å, $c = 68.55$ Å
Resolution, Å (highest shell)	42.9–3.05 (3.10–3.05)	37.4–2.65 (2.70–2.65)	30.4–3.00 (3.05–3.00)
Reflections (total/unique)	123,554/22,454	115,156/32,349	127,824/23,470
Completeness, % (highest shell)	91.7 (69.0)	99.4 (99.3)	89.2 (63.2)
$\langle I/\sigma \rangle$ (highest shell)	24.8 (4.6)	17.7 (2.2)	19.6 (2.0)
R_{sym}, % (highest shell)	4.5 (19.8)	5.6 (44.5)	5.4 (54.9)
Refinement			
R_{cryst}/R_{free}	13.2/17.8	20.3/24.6	18.5/21.0
No. of protein atoms (dimers per asymmetric unit)	2,916 (2)	5,904 (4)	2,924 (2)
No. of water molecules	0	270	0
No. of DNA atoms	1,734	—	1,734
rmsd, bond lengths, Å	0.011	0.007	0.005
rmsd, bond angles, °	1.45	1.11	0.860
Avg B-factor, $Å^2$ (protein, DNA, water)	116.5, 122.1, —	44.8, —, 37.7	76.0, 83.1, —
Stereochemistry, % (most favored, allowed, generously allowed)	96.6, 3.4, 0.0	98.4, 1.6, 0.0	95.3, 4.7, 0.0

Table S2. Sequence comparison of NolR operator sequences

Gene/operon	Sequence	Accession code
oligoAT	T**ATTAG**AGAACCCT**GAAG**TTAA	AF040724.1
oligoAA	T**ATTAG**AGAACCCT**GATG**TTAA	NA/this work
nodD1	C**GTTAG**AAAGCGCT**TAAT**TAAT	AY198324.2
nodZ	C**ATTAG**GAAGCTCT**GAAT**TGAT	AF072888.1
nolR	A**ATTAG**ACGTGATG**CATA**AAAG	AY194594.1
nodABC	T**ATTAG**AAGATGCT**CACG**TTTG	AJ302672.1
ttsI	A**TTTAG**GATTGGGT**AATA**GTCA	AF229441.2

Nucleotides in bold correspond to positions that interact with NolR in the crystal structure. Underlined nucleotides correspond to those positions identified by Vinardell et al. (1) as part of the NolR consensus motif.

1. Vinardell JM, et al. (2004) NolR regulates diverse symbiotic signals of *Sinorhizobium fredii* HH103. *Mol Plant Microbe Interact* 17(6):676–685.